Island Dynamics Model for Mound Formation: The Effect of a Step-Edge Barrier

Joe Papac,[1] Dionisios Margetis,[2] Frederic Gibou,[3] and Christian Ratsch[4]

[1]*Department of Mathematics, University of California, Los Angeles, CA 90095, USA*
[2]*Department of Mathematics, and Institute for Physical Science and Technology, and Center for Scientific Computation and Mathematical Modeling, University of Maryland, College Park, MD 20742, USA*
[3]*Department of Mechanical Engineering and Department of Computer Science and Department of Mathematics, University of California, Santa Barbara, CA 93106, USA*
[4]*Department of Mathematics and Institute for Pure and Applied Mathematics, University of California, Los Angeles, CA 90095, USA*

We formulate and implement a generalized island dynamics model of epitaxial growth based on the level-set technique to include the effect of an additional energy barrier for the attachment and detachment of atoms at step edges. For this, we invoke a mixed, Robin-type, boundary condition for the flux of adsorbed atoms (adatoms) at each step edge. In addition, we provide an analytic expression for the requisite equilibrium adatom concentration at the island boundary. The only inputs are atomistic kinetic rates. We present a numerical scheme for solving the adatom diffusion equation with such a mixed boundary condition. Our simulation results demonstrate that mounds form when the step-edge barrier is included, and that these mounds steepen as the step-edge barrier increases.

PACS numbers: 81.15.Aa, 81.15.Hi, 68.35.Ct, 68.43.Jk

I. INTRODUCTION

Epitaxial growth is of fundamental technological importance, as many modern optoelectronic devices are fabricated by this process. The various stages of epitaxial growth form a classic problem in multiscale modeling. On the one hand, the crystal surface morphology that develops is ultimately determined by the mobilities and corresponding kinetic rates of individual atoms. By definition, this consideration sets a relevant microscopic length scale of a few Ångstroms, and a typical time scale, as determined by surface diffusion in terms of a hop from one crystal lattice site to a neighboring one, of the order of 10^{-6} seconds. On the other hand, morphological features of surfaces and devices span length scales of the order of hundreds of nanometers and larger, and are grown in the laboratory within time intervals of seconds to hours. Hence, the description of epitaxial growth usually gives rise to a hierarchy of models, ranging from atomistic theories such as kinetic Monte Carlo methods, which in principle can account for every possible microscopic process, to continuum models, which may emerge from the coarse graining of individual atoms or atomic layers or atomic defects.

A significant mass transport process on crystal surfaces is the diffusion of adsorbed atoms (adatoms). If there are no surface defects, basic processes during epitaxy are the nucleation, growth, and coalescence of two-dimensional islands. Thus, close to equilibrium, homoepitaxial growth proceeds layer by layer. However, growth is far from equilibrium for many homoepitaxial systems, and, in fact, growth can become unstable and result in the formation of mounds. This kind of instability has been observed experimentally in many systems such as Cu [1, 2], Fe [3], Ag [4] and Pt [5].

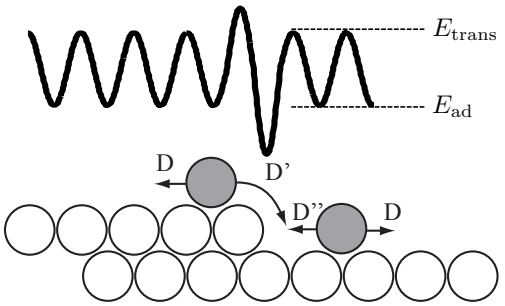

FIG. 1: Schematic representation of the step-edge barrier in the case with isotropic diffusion (when diffusion rates are scalars). The top panel shows the potential energy surface, and the bottom panel illustrates the corresponding diffusion rates near the step edge (side view).

In this paper, we formulate and numerically implement a generalized model for the dynamics of islands on crystal surfaces. The model is enriched with a condition at the island boundary that accounts for a kinetic asymmetry in the attachment and detachment of atoms at step edges (surface line defects) relative to the diffusion of adatoms on nanoscale terraces. We also express analytically an element of the prescribed boundary condition, namely, the equilibrium concentration of adatoms at the step edge. The numerical simulations that we carry out within this approach clearly demonstrate how mounds form and steepen.

The key ingredient of our generalized model is the step-edge (Ehrlich-Schwoebel, ES) energy barrier [6, 7], which is known to be the main microscopic process underly-

ing the formation of mounds. This effect is illustrated schematically in Fig. 1. By the ES barrier, an atom located next to the step-edge is more likely to diffuse to the adjacent site on the same terrace, with diffusion rate D, than diffuse downwards, to the lower terrace, with diffusion rate D'; thus, $D' < D$. Similarly, an additional barrier may exist on the lower terrace, with diffusion rate D''. The additional step-edge barrier corresponding to D' causes an uphill current and the formation of mounds, as has been shown by continuum models [8] and atomistic kinetic Monte Carlo (KMC) simulations [9]. Since this phenomenon is purely kinetic, it is often stated that mound formation is a far-from-equilibrium phenomenon. One of our goals here is to capture this out-of-equilibrium effect within the island dynamics model.

Our present work forms a nontrivial extension of a previous island dynamics model for epitaxial growth. In particular, over the last 15 years, we have developed an approach that employs the level-set technique in order to capture the kinetic processes governing island dynamics [10–14]. The model has a two-scale character, as it retains atomistic details in the growth direction (and, thus, resolves each atomic layer), but is continuous in the lateral directions (see Sec II). The parameters of this model are determined by microscopic kinetic rates. In principle, kinetic processes such as surface diffusion, edge diffusion, detachment from step-edges can be included in the model.

Because of the above features, the island dynamics model offers certain advantages over continuum approaches, e.g., [8], which cannot have atomic resolution, as well as atomistic KMC simulations, which are limited in their capability to describe macroscopic behavior of surface structures. Hence, the present approach is deemed as suitable for capturing nanoscale features of the surface morphological evolution.

In this paper we aim to describe how the effect of the ES barrier can be incorporated into the island dynamics model via a sufficiently general, Robin-type boundary condition for the adatom diffusion equation on each terrace, and study some of the consequences. Our numerics show that this additional barrier indeed leads to mound formation within the island dynamics model. For a complete treatment, we also provide a rigorous derivation of an analytic formula for the equilibrium adatom concentration near the step-edge in the presence of a microscopic step-edge barrier. In this formula, all parameters are expressed in terms of atomistic kinetic rates.

The remainder of the paper is organized as follows. In Sec. II, we describe the basic ingredients of our model and a corresponding numerical scheme that incorporates the Robin-type boundary condition for the adatom flux. Section III presents an analytic formula for the equilibrium adatom concentration, $\rho_{\rm eq}$, at the island boundary. In Sec. IV, we discuss our numerical results with focus on the prediction of mound formation. Finally, Sec. V summarizes our approach and outlines some open questions. Appendix A provides the (somewhat technical) derivation of $\rho_{\rm eq}$ on the basis of a kinetic model coupling step flow with kinks and adatoms.

II. ISLAND DYNAMICS MODEL

This section is divided into three parts. In the first part (Sec. II A), we outline the key ingredients of the island dynamics model, particularly the Robin-type boundary condition with a step-edge barrier. In the second part (Sec. II B), we describe a numerical scheme that incorporates the above boundary condition into the level-set framework. In the third part (Sec. II C), we provide a few details on the implementation of the numerical scheme.

A. Formulation: Equations of motion

The core of our approach is an island dynamics model together with a level-set method for its simulation [10–14]. Individual adatoms are not resolved explicitly within this model. Coarse-graining is invoked in the lateral directions, but atomistic detail is retained in the growth direction. Thus, the model is ideally suited to describe the evolution of nanoscale structures. The starting point is the main idea of the level-set method: For islands of height ℓ, their boundaries are described by $\Gamma_\ell = \{\mathbf{x} : \phi(\mathbf{x}) = \ell\}$, where ϕ is the level-set function which evolves according to

$$\frac{\partial \phi}{\partial t} + v_n |\nabla \phi| = 0 \ . \tag{1}$$

All physical information for the island dynamics is captured by the velocity, v_n, normal to the island boundary. This variable is given by

$$v_n = \left(\mathbf{D} \nabla \rho^- - \mathbf{D} \nabla \rho^+ \right) \cdot \mathbf{n} \ , \tag{2}$$

where $\rho(\mathbf{x}, t)$ is the adatom concentration on the terrace, $\mathbf{D}$ is the diffusion tensor, $-\mathbf{D}\nabla\rho^\pm$ is the adatom flux restricted to the island boundary in the upper $(+)$ or lower $(-)$ terrace, and $\mathbf{n}$ is the outward unit normal to the boundary. Thus, Eq. (2) is a mass conservation statement.

Within a mean-field approach, the adatom concentration, $\rho(\mathbf{x}, t)$, is obtained by solving the diffusion equation

$$\frac{\partial \rho}{\partial t} = F + \nabla \cdot (\mathbf{D} \nabla \rho) - 2 \frac{dN}{dt} + \nabla \cdot \left(\frac{\rho}{k_B T} \mathbf{D} \, \nabla E_{\rm ad} \right) \ , \tag{3}$$

where F is the external deposition flux and the last term is the thermodynamic drift ($k_B T$ is the Boltzmann energy). For simplicity, a cubic lattice with x- and y-directed diffusion is assumed, such that the diagonal entries of $\mathbf{D}$ are $D^{(x)}(\mathbf{x})$ and $D^{(y)}(\mathbf{x})$. Note, however, that a different surface geometry or diagonal diffusion can be included in the model. The term $dN/dt = \sigma_1 \langle [(D^{(x)}(\mathbf{x}) + D^{(y)}(\mathbf{x}))/2] \rho^2(\mathbf{x}) \rangle$ is the nucleation rate, where σ_1 is a capture number [15, 16] and $\langle \cdot \rangle$

denotes the average taken over all lattice sites. Stochastic elements for island nucleation [11] and the thermal dissociation of small islands [13] have been included and validated by comparison to KMC simulations [11, 13].

A few remarks on the thermodynamic drift of Eq. (3) are in order. A spatially varying, anisotropic potential energy surface is allowed, i.e., there are: (*i*) a spatially-varying adsorption energy, $E_{\rm ad}(\mathbf{x})$, and (*ii*) an anisotropic spatially varying transition energy, $E_{\rm trans}(\mathbf{x})$. The differences $E_{\rm trans}(\mathbf{x}) - E_{\rm ad}(\mathbf{x})$ define energy barriers for the diffusivities $D^{(x)}(\mathbf{x})$ and $D^{(y)}(\mathbf{x})$ (which signify surface kinetics; cf. Fig. 1). The spatial variation of $E_{\rm ad}(\mathbf{x})$ leads to a thermodynamic drift since adatoms prefer sites of lower $E_{\rm ad}$. Thus, *kinetic* and *thermodynamic* effects are properly accounted for by the model.

Equation (3) needs to be supplemented with boundary conditions at the islands' boundaries. In the absence of a step-edge barrier, the boundary condition is of the Dirichlet type, viz., [17]

$$\rho^{\pm} = \rho_{\rm eq} \ , \tag{4}$$

at the island boundary, where $\rho_{\rm eq}$ is an equilibrium adatom density at the step-edge. In contrast, in the presence of a step-edge barrier, a more general boundary condition is needed. Thus, we impose the Robin-type boundary condition

$$(\mathbf{D} - \mathbf{D}')\mathbf{n} \cdot \nabla\rho^{+} = \mathbf{n} \cdot \mathbf{D}'(\rho^{+} - \rho_{\rm eq})\mathbf{n} \ , \tag{5}$$

which must replace Eq. (4) on the upper terrace (+). In Eq. (5), $\mathbf{D}'$ is the diffusion tensor for diffusion across the step-edge and $\mathbf{n} \cdot \mathbf{D}'\mathbf{n}$ denotes the diagonal entry for $\mathbf{D}'$ for the direction normal to the boundary. We henceforth assume isotropic diffusion everywhere and thus set $\mathbf{D} = D\,\mathbf{I}$ and $\mathbf{D}' = D'\,\mathbf{I}$ where $\mathbf{I}$ is the unit tensor (unit matrix). Then, boundary condition (5) simplifies to [18]

$$\mathbf{n} \cdot \nabla\rho^{+} + \frac{D'}{D - D'}(\rho^{+} - \rho_{\rm eq}) = 0 \ , \tag{6}$$

where $D' < D$. A similar boundary condition applies to the lower terrace (−) relative to the step-edge, where D' is replaced by D''. We note in passing that as $D' \uparrow D$, condition (6) reduces to $\rho^{+} = \rho_{\rm eq}$, as it should [17].

It is worth stressing that the quantity $\rho_{\rm eq}$ entering Eq. (6) is not known a priori but can be determined from atomistic processes in the presence of a step-edge barrier. In our approach, this $\rho_{\rm eq}$ is *derived* from a kinetic model (see Sec. III and Appendix A).

B. Numerical scheme

The difficulty in solving diffusion equation (3) with boundary condition (6) and its counterpart at the lower terrace comes from the fact that points of the boundary typically do not coincide with numerical grid points, and that standard numerical approaches such as the ghost-fluid approach [19–21] cannot be used when a differential

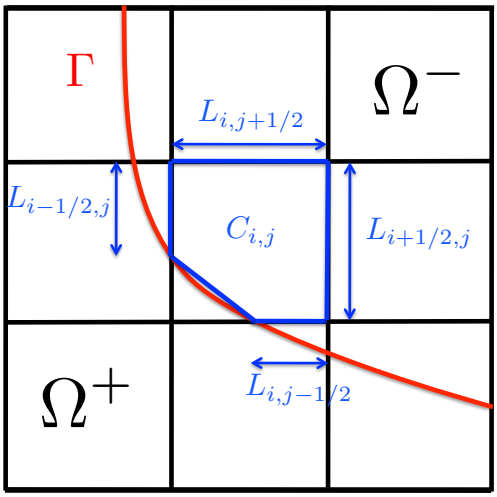

FIG. 2: (Color online) Schematic of a grid including a computational cell, $C_{i,j}$, cut by an interface curve, Γ. $\Omega_{\pm}$ corresponds to the upper (+) or lower (−) terrace, and Γ is the island boundary.

relation (and not just a value or a jump for the solution) is specified at the boundary. We have recently overcome this difficulty and have developed a finite-volume approach [22] to solve diffusion equation (3) with a boundary condition of the form (6). In the following, we describe the basic idea of our approach.

Consider a cut cell $C_{i,j}$, as depicted in Fig. 2. First, we write Eq. (3) in integral form:

$$\int_{\mathcal{C}_{i,j} \cap \Omega^{-}} \left[\frac{\partial\rho}{\partial t} - \nabla \cdot (D\nabla\rho)\right] d\Omega = \int_{\mathcal{C}_{i,j} \cap \Omega^{-}} G \, d\Omega \ , \tag{7}$$

where

$$G = F - 2\frac{dN}{dt} + \nabla \cdot \left(\frac{\rho}{k_B T} D(\nabla E_{\rm ad})\right) \ .$$

We then apply an implicit scheme in time, expressing Eq. (7) as

$$\int_{\mathcal{C}_{i,j} \cap \Omega^{-}} \tilde{\mathcal{L}}^{-} \rho^{n+1} \, d\Omega = \int_{\mathcal{C}_{i,j} \cap \Omega^{-}} \left(\tilde{\mathcal{L}}^{+} \rho^{n} - \Delta t \tilde{G}^{n}\right) d\Omega \ , \tag{8}$$

where $\tilde{G}$ is an approximation of G, $\tilde{\mathcal{L}}$ is a second-order central-difference approximation of the linear operator

$$\mathcal{L}^{\pm} = \left(I \pm \frac{\Delta t}{2} \nabla \cdot (D\nabla)\right) ,$$

and ρ^{n} denotes the value of the solution ρ at time $t = t^{n}$. Equation (8) is a discretized-in-time version of Eq. (7).

The main difficulty in approximating Eq. (8) is the evaluation of the term

$$\int_{\mathcal{C}_{i,j} \cap \Omega^{-}} \left[I - \frac{\Delta t}{2} \nabla \cdot (D\nabla)\right] \rho^{n+1} \, d\Omega \ ,$$

in such a way as to impose Robin boundary condition (6). Referring to Fig. 2, which depicts the general case of a cell $\mathcal{C}_{i,j}$ cut by the interface Γ, the term $\int_{\mathcal{C}_{i,j}\cap\Omega^-}\rho^{n+1}\,d\Omega$ can be approximated as

$$\int_{\mathcal{C}_{i,j}\cap\Omega^-}\rho^{n+1}\,d\Omega=\rho_{i,j}^{n+1}\cdot[\text{Area of }(\mathcal{C}_{i,j}\cap\Omega^-)]\ .$$

The respective approximation of the term $\int_{\mathcal{C}_{i,j}\cap\Omega^-}\nabla\cdot(D\nabla)\rho^{n+1}\,d\Omega$ is achieved by first applying the divergence theorem and thus rewriting the requisite surface integral in an equivalent form involving line integrals:

$$\begin{aligned}\int_{\partial(\mathcal{C}_{i,j}\cap\Omega^-)}D\nabla\rho^{n+1}\cdot\mathbf{n}\,dl=&\int_{\partial\mathcal{C}_{i,j}\cap\Omega^-}D\nabla\rho^{n+1}\cdot\mathbf{n}\,dl\\&+\int_{\mathcal{C}_{i,j}\cap\Gamma}D\nabla\rho^{n+1}\cdot\mathbf{n}\,dl\ .\end{aligned}\tag{9}$$

The first term on the right-hand side of Eq. (9) is approximated by a standard finite difference scheme:

$$\begin{aligned}\int_{\partial\mathcal{C}_{i,j}\cap\Omega^-}\nabla\rho^{n+1}\cdot\mathbf{n}\,dl\ =&\frac{\rho_{i+1,j}^{n+1}-\rho_{i,j}^{n+1}}{\Delta x}\ L_{i+\frac{1}{2},j}\\&-\frac{\rho_{i,j}^{n+1}-\rho_{i-1,j}^{n+1}}{\Delta x}L_{i-\frac{1}{2},j}\\&+\frac{\rho_{i,j+1}^{n+1}-\rho_{i,j}^{n+1}}{\Delta y}L_{i,j+\frac{1}{2}}\\&-\frac{\rho_{i,j}^{n+1}-\rho_{i,j-1}^{n+1}}{\Delta y}L_{i,j-\frac{1}{2}}\ ,\end{aligned}\tag{10}$$

where $\rho_{i,j}^{n+1}$ is the value of the solution ρ at some point in $\mathcal{C}_{i,j}$ at time t^{n+1}, $L_{i\pm1/2}$ (resp., $L_{j\pm1/2}$) denotes the length of the face in Ω^- between i and $i\pm1$ (resp., j and $j\pm1$), as depicted in Fig. 2 (right part of the cell). On the other hand, the second term on the right-hand side of Eq. (9), which amounts to the flux normal the boundary Γ, explicitly invokes the Robin boundary condition (6):

$$\int_{\mathcal{C}_{i,j}\cap\Gamma}\nabla\rho^{n+1}\cdot\mathbf{n}\,dl=\int_{\mathcal{C}_{i,j}\cap\Gamma}-\frac{D'}{D-D'}(\rho_{i,j}^{n+1}-\rho_{\rm eq})\,dl\ .$$

The requisite integrals are approximated by the methods of Min and Gibou [23, 24]. In [22], it was rigorously shown that the solution is accurate to second order in the mesh size and leads to a symmetric linear system that can be efficiently inverted with a preconditioned conjugate gradient method [25].

C. Some implementation details

In addition to the ES barrier, a few physical corrections were implemented in our code to account for very thin regions in which there may be only one or two grid points per layer in each direction. This scenario is not a problem in the absence of a step-edge barrier (when we have a Dirichlet boundary condition for ρ), because we prescribe the adatom density at the step-edge to be equal to the equilibrium adatom density, $\rho_{\rm eq}$. In this case, even with just a single grid point on a narrow terrace, we can still calculate the gradients of ρ because $\rho_{\rm eq}$ is prescribed. In contrast, with a step-edge barrier, when Robin condition (6) is imposed, we do not have an explicit value of ρ prescribed at the boundary. Then, we need at least three grid nodes per terrace in each direction in order to calculate the gradients of ρ, which determine the normal velocity of the step-edge according to Eq. (2).

In typical simulations with a large step-edge barrier, i.e., when $D'\ll D$, very thin terraces are often visible and multiple layers are often developed between two neighboring grid nodes. To capture the correct physical behavior, we apply the following approximation: When we have fewer than three grid nodes on a narrow terrace, we assume that all flux deposited onto that small area will be added to the boundary, instead of calculating the flux into the boundary from gradients of ρ [cf. Eq. (2)]. More precisely, we assume that half of the mass is added to the lower terrace, and the other half to the upper terrace.

The second physical approximation that we utilize is concerned with areas in which a jump of multiple terrace levels occurs within two neighboring grid nodes. When we have this situation, we divide the calculated velocity contribution by the difference in height between grid nodes. Essentially, we are enforcing conservation of mass by assuming that equal amounts of flux are deposited onto each layer.

Finally, we note that in our present numerical simulations we use $\nabla E_{\rm ad}=0$ (no thermodynamic drift), in the presence of isotropic diffusion. The results are discussed in Sec. IV.

III. EQUILIBRIUM ADATOM DENSITY, $\rho_{\rm eq}$

In this section, we provide a formula for the $\rho_{\rm eq}$ of Eq. (6) in the presence of a step-edge barrier. This formula stems from a terrace-step-kink (TSK) model, which couples step flow with the motion of kinks and adatoms along step-edges and retains atomistic information in the requisite kinetic rates [26]. Our detailed, somewhat general, calculation of $\rho_{\rm eq}$ can be found in Appendix A. Here, we simplify the derived expression for $\rho_{\rm eq}$ by restricting attention to parameters used in the simulations that will be presented in this paper.

First, we briefly describe the setting of the TSK model [26]. The geometry consists of a periodic sequence of steps with atomic height a separated by distance L as they move along a fundamental crystallographic axis. Atoms hop on each terrace and attach/detach to/from step-edges. Atomistic kinetic rates are invoked to describe the related transitions. Here, we use the notation introduced in [26]. In particular, $D_{\rm T}=D$ is the terrace

(T) adatom diffusion coefficient, $D^+_{\rm TE} = D'$ amounts to transitions from the upper (+) terrace to the step-edge (E) and $D^-_{\rm TE} = D''$ refers to transitions from the lower (−) terrace to the edge; $D^-_{\rm ET} = \mathfrak{D}$ is the rate for the transition from the step-edge to the lower terrace and $D^+_{\rm ET}$ is the transition rate from the edge to the upper, terrace and by detailed balance $D^+_{\rm ET} = \mathfrak{D}D'/D''$; $D_{\rm EK} = D_{\rm E}$ corresponds to hopping from the step-edge (E) to kinks (K); $D^+_{\rm TK} = D'$ refers to transitions from the upper terrace (T) to kinks (K) and $D^-_{\rm TK} = D''$ describes transitions from the lower terrace to kinks; and $D_{\rm EB} = D_{\rm E}$, $D^+_{\rm TB} = D'$ and $D^-_{\rm TB} = D''$ correspond to transitions from the step-edge (E) or terrace (T) to the bulk (B) of atoms. The constant $D_{\rm E}$ is the step-edge diffusion coefficient. Note that $D^+_{\rm ET}D^-_{\rm TE} = D^+_{\rm TE}D^-_{\rm ET}$, as dictated by detailed balance [26].

From the TSK model, it can generally be shown that (see Appendix A)

$$\rho_{\rm eq} \approx \mathcal{C}\left[\frac{FL}{2}\frac{1}{c_{w1}D_{\rm EK} + \mathcal{C}(c_{w2}D^+_{\rm TK} + c_{w3}D^-_{\rm TK})}\right]^{2/3} \times \left[\frac{c_{h1}D_{\rm EB} + \mathcal{C}(c_{h2}D^+_{\rm TB} + c_{h3}D^-_{\rm TB})}{c_{g1}D_{\rm EK} + \mathcal{C}(c_{g2}D^+_{\rm TK} + c_{g3}D^-_{\rm TK})}\right]^{1/3}, \tag{11}$$

where

$$\mathcal{C} = \frac{\dfrac{a}{L}\left(c_{f+}\dfrac{D^+_{\rm ET}}{D_{\rm T}} + c_{f-}\dfrac{D^-_{\rm ET}}{D_{\rm T}}\right) + c_{f+}c_{f-}\dfrac{\Lambda}{D^2_{\rm T}}}{\dfrac{a}{L}\left(c_{f+}\dfrac{D^+_{\rm TE}}{D_{\rm T}} + c_{f-}\dfrac{D^-_{\rm TE}}{D_{\rm T}}\right) + c_{f+}c_{f-}\dfrac{D^+_{\rm TE}}{D_{\rm T}}\dfrac{D^-_{\rm TE}}{D_{\rm T}}}, \tag{12}$$

and $\Lambda = D^-_{\rm TE}D^+_{\rm ET} = D^+_{\rm TE}D^-_{\rm ET}$. The constants $c_{f\pm}$, c_{wj}, c_{gj} and c_{hj} ($j = 1, 2, 3$) are coordination numbers for related transition paths within a mean field description (see Appendix A), with values $c_{f+} = c_{f-} = 1$, $c_{w1} = c_{w2} = 2$, $c_{w3} = 1$, $c_{g1} = c_{g3} = 2$, $c_{g2} = 4$, $c_{h1} = 2$, $c_{h2} = 3$, $c_{h3} = 1$ [26].

The use of the above numerical values and the parameters D, $D_{\rm E}$, D', D'', $\mathfrak{D}$ into Eqs. (11) and (12) yields $\mathcal{C} = \mathfrak{D}/D''$, and

$$\rho_{\rm eq} \approx 2^{-2/3}a^{-2}P_e^{2/3}\frac{\mathfrak{D}}{D''}\left[\frac{D_{\rm E}}{2D_{\rm E} + (2D'/D'' + 1)\mathfrak{D}}\right]^{2/3} \times \left[\frac{2D_{\rm E} + (3D'/D'' + 1)\mathfrak{D}}{2D_{\rm E} + (4D'/D'' + 2)\mathfrak{D}}\right]^{1/3}, \tag{13}$$

where $P_e = FLa^3/D_{\rm E}$ is the edge Péclet number. Equation (13) can be further simplified by elimination of the step-edge barrier in the lower terrace, setting $D'' \approx D$.

IV. NUMERICAL RESULTS AND DISCUSSION

The main results of our model are shown in Fig. 3. These are snapshots of typical island dynamics simulations after the deposition of approximately 32 monolayers for different values of the step-edge barrier, i.e., different values of D'/D. We assume that there is no step-edge barrier for atoms that attach to the step-edge from the lower terrace, and thus set $D'' = D$. Furthermore, we assume that $E_{\rm ad}$ is a constant everywhere (thus, $\nabla E_{\rm ad} = 0$). All simulations were carried out with a set of typical growth parameters, and we chose a deposition rate $F = 1.0$ MLs^{-1}, a diffusion rate $D = 10^6$ s^{-1}, an adatom detachment rate $\mathfrak{D} = 10$ s^{-1}, a lattice size of 132 lattice sites, and a numerical resolution of 192 grid points in each spatial direction. We obtained qualitatively similar results for different growth parameters.

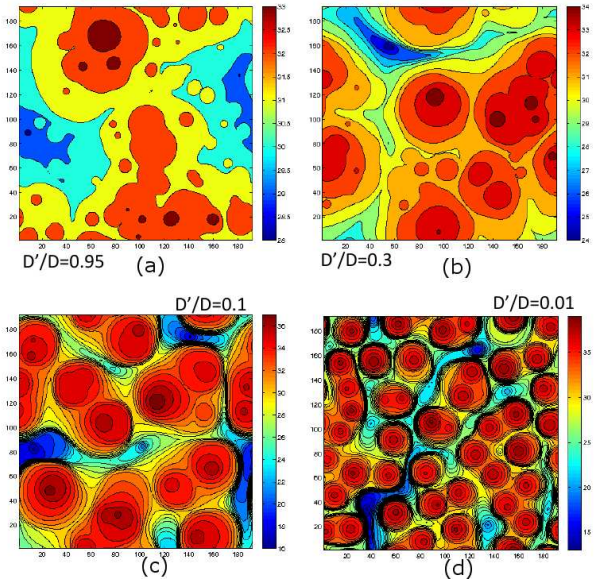

FIG. 3: (Color online) Island morphology after the deposition of 32 atomic layers for different values of D'/D. (a) $D'/D = 0.95$ (nearly no step-edge barrier); (b) $D'/D = 0.3$; (c) $D'/D = 0.1$; and (d) $D'/D = 0.01$ (large step-edge barrier). The steepening of mounds for decreasing values of D'/D (increasing step-edge barrier) is evident.

When there is no step-edge barrier (or a small step-edge barrier), growth proceeds essentially layer by layer, and there are only a few exposed layers present [cf. Fig. 3(a)]. As the step-edge barrier increases ($D'/D = 0.3$ and $D'/D = 0.1$, in Figs. 3(b) and (c), respectively], growth starts becoming unstable, and more and more layers are exposed. In Fig. 3(d) we have a substantial step-edge barrier ($D'/D = 0.01$), and we observe steep mounds with over 20 exposed layers in our simulations.

The transition from layer-by-layer growth to unstable growth and the formation of mounds can also be viewed in Fig. 4, where we show the time evolution of the surface roughness, w, for the above four different values of D'/D. The surface roughness is defined by $w = \sqrt{\langle (h_i - \langle h \rangle)^2 \rangle}$, where h_i is the height at lattice site i and the average $\langle \cdot \rangle$ is taken over all lattice sites. Evidently, when D'/D is close to unity [cf. Fig. 4(a)], the roughness oscillates, which is a typical signature of layer-by-layer growth. As

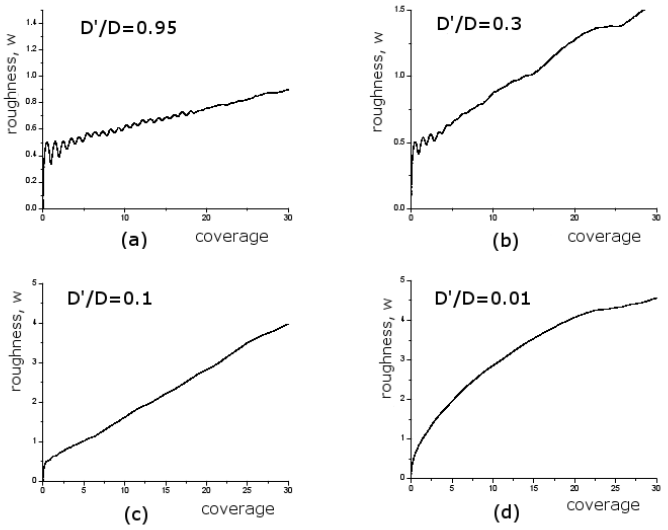

FIG. 4: Time evolution of the surface roughness, $w = [\langle (h_i - \langle h \rangle)^2 \rangle]^{1/2}$, for different values of D'/D. (a) $D'/D = 0.95$ (small step-edge barrier); (b) $D'/D = 0.3$; (c) $D'/D = 0.1$; and (d) $D'/D = 0.01$ (large step-edge barrier). As the step-edge barrier increases, w increases considerably and oscillations of w as a function of time die out.

D'/D decreases, the oscillations of w as a function of time (or, coverage) die out. Indeed, no such oscillations of w are visible in our simulations for $D'/D = 0.1$ and $D'/D = 0.01$ [cf. Figs. 4(c), (d)]. Notably, as D'/D decreases, the surface roughness increases substantially.

Our treatment of island dynamics is amenable to extensions in order to model mound formation in more realistic settings. In laboratory experiments, it is often observed that the mounds get steeper as they form, until they reach a final slope. This slope selection has been explained via (atomistic) KMC simulations [9], as well as by continuum step dynamics models [27] through a mechanism called downward funneling. By this mechanism, atoms that are deposited close to a step-edge are more likely to be incorporated into the lower terrace: they are "funneled" toward the lower terrace. As long as the upper terrace is large, this effect is small. However, as the upper terrace gets narrower (which happens when the mound gets steeper), the relative importance of this effect increases, and eventually this effective downward flux balances the effective upward flux due to a step-edge barrier.

In our simulations we have not incorporated downward funneling, and as a result, we do not observe a slope selection. In fact, the mounds shown in Fig. 3 steepen continuously, until they reach a slope that is determined by the numerical resolution of our simulation. In principle, it is possible to incorporate downward funneling in our approach. This additional effect is the subject of work in progress. Another effect missing from our island dynamics model is that of elastic step-step interactions. In particular, the inclusion of step-step interactions in our model and the study of their influence on slope selection are currently under investigation.

V. SUMMARY AND OUTLOOK

In this paper, we substantially improved and numerically simulated an island dynamics model, combined with a level-set approach, in order to study mound formation and evolution on crystal surfaces. In particular, we included and implemented an additional step-edge barrier by applying a general, Robin-type boundary condition for the adatom flux normal to the step-edge. We also introduced a stable, second-order accurate numerical scheme that enables us to solve the adatom diffusion equation with such a boundary condition on a fixed grid with moving interfaces.

The Robin-type boundary condition of our generalized model contains the equilibrium adatom density, $\rho_{\rm eq}$, at the step-edge as a key parameter. Here, we presented an analytic formula for $\rho_{\rm eq}$, which we rigorously derived from an atomistic, kinetic model of epitaxial growth that couples step flow with the motion of kinks and diffusion of adatoms. This formula expresses $\rho_{\rm eq}$ in terms of atomistic transition rates.

The inclusion of a step-edge barrier in the model leads to the formation of mounds. Our numerical simulations demonstrate how mounds form and steepen as a result of the increase of the step-edge barrier. In order to obtain the experimentally observed selection of slopes of the mounds, additional physics needs to be included in the model. This will be part of our future work.

ACKNOWLEDGMENTS

DM's work was supported by the NSF via Grant No. DMS 08-47587. The research of FG was supported in part by ONR N00014-11-1-0027, NSF CHE 1027817 and by the W.M. Keck Foundation. JP and CR acknowledges financial support from the NSF under grant CHE-1027797.

APPENDIX A: KINETIC DERIVATION OF $\rho_{\rm eq}$

In this appendix, we determine the $\rho_{\rm eq}$ entering Robin boundary condition (6), in the presence of a step-edge barrier, by starting with the kinetic formulation of [26]. Our derivation forms a nontrivial modification of an earlier calculation of $\rho_{\rm eq}$ where effects of step-edge barriers are left out [26].

In the spirit of [26], we focus on the kinetic steady state of a periodic array of steps with atomic height a separated by distance L as they move at velocity v along

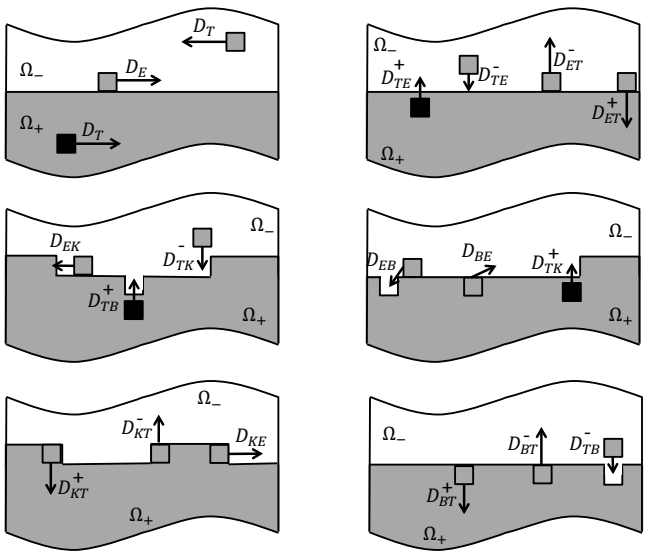

FIG. 5: Schematic of microscopic processes near a straight step edge according to the terrace-step-kink model of [26]. The relevant kinetic, transition rates are shown by use of arrows. $\Omega_\pm$ denotes the upper (+) or lower (−) terrace.

a fundamental crystallographic (say, x-) direction. Suppose the steps are descending in the positive x-direction. We consider homogeneous, isotropic terrace diffusion of constant scalar diffusion coefficient $D_{\rm T}$, with $\nabla E_{\rm ad} \equiv 0$ in the absence of nucleation ($dN/dt \equiv 0$). The diffusion equation for the adatom density, ρ, on each terrace reads

$$\frac{\partial \rho}{\partial t} = F + D_{\rm T}\,\nabla^2 \rho. \tag{A1}$$

In the kinetic steady state, the adatom density is a traveling wave, $\rho = \varrho(x - vt)$ where $\varrho(\xi)$ is smooth. Thus, Eq. (A1) is solved by $\varrho(\xi) = c_1 e^{-v\xi/D_{\rm T}} - (F/v)\xi + c_2$ where $0 < \xi < L$, $\xi = x - vt$, and c_1 and c_2 are integration constants to be determined. By periodicity of the step train, the adatom densities at each step-edge on the upper (+) and lower (−) terrace are:

$$\begin{aligned} \rho_+ &= \varrho(L) = c_1 e^{-vL/D_{\rm T}} - (F/v)L + c_2, \\ \rho_- &= \varrho(0) = c_1 + c_2, \end{aligned} \tag{A2}$$

by which we can express c_1 and c_2 in terms of ρ_+ and ρ_-, e.g., $c_2 = (1 - e^{-vL/D_{\rm T}})^{-1}(\rho_+ - \rho_- e^{-vL/D_{\rm T}} + FL/v)$.

We need to determine $\rho_\pm = \rho_{{\rm eq},\pm}$ in terms of the requisite atomistic kinetic rates. For this purpose, we will invoke the edge-adatom density, ϕ, and kink density, k, which are constants in the kinetic steady state. The relevant microscopic processes and transition rates are shown in Fig. 5.

First, we relate $\rho_\pm$ to ϕ. Denoting $f_\pm$ the mass fluxes toward the step-edge in the normal direction, we impose the kinetic relation [26] $f_- = v\rho_- + D_{\rm T}(\partial_\xi \varrho)_- = vc_2 - D_{\rm T}F/v$ at $\xi = 0$, where $\partial_\xi = \partial/\partial\xi$. By global mass conservation, $f_+ + f_- = LF$. By solving the last two equations for f_+ and f_- and using Eq. (A2), we obtain

$$f_- = \frac{v(\rho_+ - \rho_- e^{-vL/D_{\rm T}}) + FL}{1 - e^{-vL/D_{\rm T}}} - \frac{D_{\rm T}F}{v}, \tag{A3}$$

with $f_+ = Fl - f_-$ and $v = a^2(f_- + f_+) = a^2 FL$.

To relate $\rho_\pm$ to ϕ, we now apply the mean field approximation [26] $f_\pm = c_{f\pm}(D^\pm_{\rm TE} a\rho_\pm - D^\pm_{ET}\phi)a^{-2}$, where $D^\pm_{\rm TE}$ and $D^\pm_{\rm ET}$ are diffusion coefficients for the transition of atoms hopping from the upper (+) or lower (−) terrace (T) to the edge (E) and vice versa, and $c_{f\pm}$ are associated coordination numbers. By combining the mean field relation for $f_\pm$ with Eq. (A3) and $f_+ = FL - f_-$, we derive a system of equations for ρ_+ and ρ_- (given ϕ):

$$\begin{aligned} &\frac{v}{1 - e^{-vL/D_{\rm T}}}\rho_+ - \left(\frac{ve^{-vL/D_{\rm T}}}{1 - e^{-vL/D_{\rm T}}} + c_{f-} D^-_{\rm TE} a^{-1}\right)\rho_- \\ &= \frac{D_{\rm T}F}{v} - \frac{FL}{1 - e^{-vL/D_{\rm T}}} - c_{f-} D^-_{ET}\phi a^{-2}, \end{aligned} \tag{A4}$$

$$\begin{aligned} &\left(c_{f+} D^+_{\rm TE} a^{-1} + \frac{v}{1 - e^{-vL/D_{\rm T}}}\right)\rho_+ - \frac{ve^{-vL/D_{\rm T}}}{1 - e^{-vL/D_{\rm T}}}\rho_- \\ &= \frac{D_{\rm T}F}{v} - FL\frac{e^{-vL/D_{\rm T}}}{1 - e^{-vL/D_{\rm T}}} + c_{f+} D^+_{\rm ET}\phi a^{-2}. \end{aligned} \tag{A5}$$

The solution of this system yields $\rho_\pm$ in terms of ϕ. We simplify the resulting formulas by assuming small convection, i.e., $vL/D_{\rm T} \ll 1$ so that $1 - e^{-vL/D_{\rm T}} \approx vL/D_{\rm T}$, along with

$$\frac{a}{L} \ll \left[\frac{a}{L}\left(\frac{c_{f+}}{P_{e+}} + \frac{c_{f-}}{P_{e-}}\right) + \frac{D^\pm_{\rm TE}}{D_{\rm T}}\frac{c_{f+}c_{f-}}{P_{e\mp}}\right] a\phi,$$

where $P_{e\pm} = a^3 FL/D^\pm_{\rm ET}$ is the edge Péclet number with reference to the upper (+) or lower (−) terrace; in many physical situations of interest, $P_{e\pm} \ll 1$. Consequently, Eqs. (A4) and (A5) give

$$\rho_\pm \approx \mathcal{C}_\pm\, a^{-1}\phi, \tag{A6}$$

where

$$\mathcal{C}_\pm = \frac{\dfrac{a}{L}\left(c_{f+}\dfrac{D^+_{\rm ET}}{D_{\rm T}} + c_{f-}\dfrac{D^-_{\rm ET}}{D_{\rm T}}\right) + c_{f+}c_{f-}\dfrac{D^\mp_{\rm TE}}{D_{\rm T}}\dfrac{D^\pm_{\rm ET}}{D_{\rm T}}}{\dfrac{a}{L}\left(c_{f+}\dfrac{D^+_{\rm TE}}{D_{\rm T}} + c_{f-}\dfrac{D^-_{\rm TE}}{D_{\rm T}}\right) + c_{f+}c_{f-}\dfrac{D^+_{\rm TE}}{D_{\rm T}}\dfrac{D^-_{\rm TE}}{D_{\rm T}}}. \tag{A7}$$

At this stage, we should point out that Eqs. (A6) and (A7) can be further simplified. By the principle of detailed balance, the rates $D^\pm_{\rm ET}$ and $D^\pm_{\rm TE}$ satisfy [26]

$$D^+_{\rm ET} D^-_{\rm TE} = D^+_{\rm TE} D^-_{\rm ET}. \tag{A8}$$

It follows that $\mathcal{C}_+ = \mathcal{C}_- \equiv \mathcal{C}$. Thus, we establish that

$$\rho_+ \approx \rho_- \approx \rho_{\rm eq} \approx \mathcal{C}\, a^{-1}\phi, \tag{A9}$$

where $\mathcal{C}$ is given by Eq. (A7) independent of subscript. It remains to compute ϕ.

Next, we determine a relation between ϕ and the kink density, k. Apply the geometric law [26] $a^2FL = v = awk$, where w is the kink mean velocity. This w satisfies the mean field equation $w = w_1 + w_2 + w_3$, where $w_1 = c_{w1}(D_{\rm EK}\phi - D_{\rm KE}a^{-1})$, $w_2 = c_{w2}(D^+_{\rm TK}a\rho_+ - D^+_{\rm KT}a^{-1})$, and $w_3 = c_{w3}(D^-_{\rm TK}a\rho_- - D^-_{\rm KT}a^{-1})$. In these mean field laws, $D_{\rm EK}$, $D_{\rm KE}$, $D^\pm_{\rm TK}$ and $D^\pm_{\rm KT}$ are diffusion coefficients for transitions from an edge (E) to a kink (K) and vice versa, and from the upper or lower terrace (T) to a kink and vice versa. Furthermore, c_{wj} ($j = 1, 2, 3$) are coordination numbers for these transitions. Accordingly, we find

$$\frac{aFL}{k} \approx c_{w1}D_{\rm EK}\phi + c_{w2}D^+_{\rm TK}a\rho_+ + c_{w3}D^-_{\rm TK}a\rho_-, \quad \text{(A10)}$$

by neglecting the effects of $D_{\rm KE}$ and $D^\pm_{\rm KT}$. Equations (A9) and (A10) yield a relation between ϕ and k:

$$k\phi \approx aFL[c_{w1}D_{\rm EK} + \mathcal{C}(c_{w2}D^+_{\rm TK} + c_{w3}D^-_{\rm TK})]^{-1}. \quad \text{(A11)}$$

Another relation for ϕ and k is obtained via the transport law for kinks [26], $\partial_t k + \partial_s[w(k_r - k_l)] = 2(g - h)$ where k_r (k_l) is the density of right- (left-) facing kinks, $k_r = k_l = k/2$ for straight edges along the x-axis, g is the net gain in kink pairs due to nucleation/breakup, and h is the net loss of kink pairs (s: edge arc length). For constant k, we must impose $g = h$; and replace the source terms g and h by known mean field expressions [26].

In particular, we write $g = g_1+g_2+g_3$ and $h = h_1+h_2+h_3$ with the following mean field laws for g_j and h_j [26]: $g_1 = c_{g1}(D_{\rm EK}\phi^2 - D_{\rm KE}k_rk_l)a^{-1}$, $g_2 = c_{g2}(D^+_{\rm TK}a\rho_+\phi - D^+_{\rm KT}k_rk_l)a^{-1}$, and $g_3 = c_{g3}(D^-_{\rm TK}a\rho_-\phi - D^-_{\rm KT}k_rk_l)a^{-1}$; in addition, $h_1 = c_{h1}(D_{\rm EB}\phi k_rk_l - D_{\rm BE}a^{-3})$, $h_2 = c_{h2}(D^+_{\rm TB}a\rho_+k_rk_l - D^+_{\rm BT}a^{-3})$, $h_3 = c_{h3}(D^-_{\rm TB}a\rho_-k_rk_l - D^-_{\rm BT}a^{-3})$, where $D_{\rm EB}$, $D_{\rm BE}$, $D^\pm_{\rm TB}$ and $D^\pm_{\rm BT}$ are suitable diffusion coefficients for atom transitions from the edge (E) to the bulk (B) and vice versa, and from the terrace (T) to the bulk and vice versa. Furthermore, c_{gj} and c_{hj} are associated coordination numbers. Therefore, setting $g = h$ leads to an algebraic equation for ϕ, k and $\rho_\pm$:

$$\begin{aligned} &c_{g1}D_{\rm EK}\phi^2 + c_{g2}D^+_{\rm TK}a\rho_+\phi + c_{g3}D^-_{\rm TK}a\rho_-\phi)a^{-1} \\ &= (c_{h1}D_{\rm EB}\phi + c_{h2}D^+_{\rm TB}a\rho_+ + c_{h3}D^-_{\rm TB}a\rho_-)k^2. \end{aligned} \quad \text{(A12)}$$

In our derivation of the last relation, we neglected terms proportional to $D_{\rm KE}$, $D^\pm_{\rm KT}$, $D_{\rm BE}$ and $D^\pm_{\rm BT}$. The combination of Eqs. (A9) and (A12) yields

$$\phi \approx \frac{1}{4}\,\frac{c_{h1}D_{\rm EB} + \mathcal{C}(c_{h2}D^+_{\rm TB} + c_{h3}D^-_{\rm TB})}{c_{g1}D_{\rm EK} + \mathcal{C}(c_{g2}D^+_{\rm TK} + c_{g3}D^-_{\rm TK})}ak^2. \quad \text{(A13)}$$

The last stage of our calculation involves the solution of the system of Eqs. (A11) and (A13) for ϕ and k. Thus, we obtain

$$\begin{aligned} \phi \approx a&\left[\frac{FL}{2}\,\frac{1}{c_{w1}D_{\rm EK} + \mathcal{C}(c_{w2}D^+_{\rm TK} + c_{w3}D^-_{\rm TK})}\right]^{2/3} \\ &\times\left[\frac{c_{h1}D_{\rm EB} + \mathcal{C}(c_{h2}D^+_{\rm TB} + c_{h3}D^-_{\rm TB})}{c_{g1}D_{\rm EK} + \mathcal{C}(c_{g2}D^+_{\rm TK} + c_{g3}D^-_{\rm TK})}\right]^{1/3} \end{aligned} \quad \text{(A14)}$$

and

$$\begin{aligned} k \approx &\left[\frac{4FL}{c_{w1}D_{\rm EK} + \mathcal{C}(c_{w2}D^+_{\rm TK} + c_{w3}D^-_{\rm TK})}\right]^{1/3} \\ &\times\left[\frac{c_{g1}D_{\rm EK} + \mathcal{C}(c_{g2}D^+_{\rm TK} + c_{g3}D^-_{\rm TK})}{c_{h1}D_{\rm EB} + \mathcal{C}(c_{h2}D^+_{\rm TB} + c_{h3}D^-_{\rm TB})}\right]^{1/3}. \end{aligned} \quad \text{(A15)}$$

Equations (A9) and (A14) lead to the desired formula for $\rho_{\rm eq}$, Eq. (11).

In the special case without a step-edge barrier, we set $D^\pm_{\rm TE} = D^\pm_{\rm TK} = D^\pm_{\rm TB} = D_{\rm T}$ and $D^\pm_{\rm ET} = D_{\rm EK} = D_{\rm EB} = D_{\rm E}$ [26]. Then, we have $\mathcal{C} = D_{\rm E}/D_{\rm T}$, and Eqs. (A9), (A14) and (A15) give $\rho_{\rm eq} \approx (D_{\rm E}/D_{\rm T})a^{-1}\phi$, $\phi = (3/16)^{1/3}5^{-2/3}a^{-1}\,P_e^{2/3}$ and $k = (16/15)^{1/3}a^{-1}P_e^{1/3}$, where $P_e = FLa^3/D_{\rm E} = P_{e+} = P_{e-}$ (edge Péclet number); cf. Eqs. (7.3)–(7.5) in [26].

[1] H.-J. Ernst, F. Fabre, R. Folkerts, and J. Lapujoulade, Phys. Rev. Lett. **72**, 112 (1994).
[2] J.-K. Zuo and J. F. Wendelken, Phys. Rev. Lett. **78**, 2791 (1997).
[3] J. A. Stroscio, D. T. Pierce, M. D. Stiles, A. Zangwill, and L. M. Sander, Phys. Rev. Lett. **75**, 4246 (1995).
[4] J. Wollschläger, E. Z. Luo, and M. Henzler, Phys. Rev. B **57**, 15541 (1998).
[5] M. Bott, T. Michely, and G. Comsa, Surf. Sci. **272**, 161 (1992).
[6] G. Ehrlich and F. Hudda, J. Chem. Phys. **44**, 1039 (1966).
[7] R. L. Schwoebel and E. J. Shipsey, J. Appl. Phys. **37**, 3682 (1966).
[8] J. Villain, J. Phys. (France) I **1**, 19 (1991).
[9] P. Šmilauer and D. D. Vvedensky, Phys. Rev. B **52**, 14263 (1995).
[10] R. E. Caflisch, M. F. Gyure, B. Merriman, S. Osher, C. Ratsch, D. D. Vvedensky, and J. J. Zinck, Appl. Math. Lett. **12**, 13 (1999).
[11] C. Ratsch, M. F. Gyure, S. Chen, M. Kang, and D. D. Vvedensky, Phys. Rev. B **61**, R10598 (2000).
[12] S. Chen, B. Merriman, M. Kang, R. E. Caflisch, C. Ratsch, L.-T. Cheng, M. Gyure, R. P. Fedkiw, C. Anderson, and S. Osher, J. Comput. Phys. **167**, 475 (2001).
[13] M. Petersen, C. Ratsch, R. E. Caflisch, and A. Zangwill, Phys. Rev. E **64**, 061602 (2001).
[14] X. Niu, R. Vardavas, R. E. Caflisch, and C. Ratsch, Phys. Rev. B **74**, 193403 (2006).
[15] G. S. Bales and D. C. Chrzan, Phys. Rev. B **50**, 6057 (1994).
[16] F. Gibou, C. Ratsch, and R. E. Caflisch, Phys. Rev. B

67, 155403 (2003).
[17] W. K. Burton, N. Cabrera, and F. C. Frank, Philos. Trans. R. Soc. London Ser. A **243**, 299 (1951).
[18] A. Pimpinelli and J. Villain, *Physics of Crystal Growth* (Cambridge University Press, Cambridge, UK, 1999).
[19] X. D. Liu, R. Fedkiw, and M. Kang, J. Comput. Phys. **154**, 151 (2000).
[20] F. Gibou, R. Fedkiw, L.-T. Cheng, and M. Kang, J. Comput. Phys. **176**, 205 (2002).
[21] F. Gibou and R. Fedkiw, J. Comput. Phys. **202**, 577 (2005).
[22] J. Papac, F. Gibou, and C. Ratsch, J. Comput. Phys. **229**, 875 (2010).
[23] C. Min and F. Gibou, J. Comput. Phys. **227**, 9686 (2008).
[24] C. Min and F. Gibou, J. Comput. Phys. **226**, 1432 (2007).
[25] Y. Saad, *Iterative Methods for Sparse Linear Systems* (PWS Publishing, Boston, MA, 1996).
[26] R. E. Caflisch, W. E., M. F. Gyure, B. Merriman, and C. Ratsch, Phys. Rev. E **59**, 6879 (1999).
[27] M. Li and J. W. Evans, Phys. Rev. Lett. **95**, 256101 (2005).